Pergamon

Int. J. Heat Mass Transfer. Vol. 39, No. 14, pp. 2895–2906, 1996

0017-9310/96 $15.00 + 0.00

0017-9310(95)00384-3

Thermovibrational convection in a vertical cylinder

FRANK T. FERGUSON
Code 691, NASA-Goddard Space Flight Center, Greenbelt, MD 30771, U.S.A.

and

LEMBIT U. LILLELEHT
Department of Chemical Engineering, University of Virginia, Charlottesville, VA 22903, U.S.A.

(*Received* 7 *August* 1995 *and in final form* 24 *October* 1995)

Abstract—We have completed a study of thermovibrational convection in a vertical, cylindrical cavity for Rayleigh numbers, Ra, of 0, 10^4 and 10^5, and vibrational Grashof numbers, Gr_v, of 10^5 and 10^6. Results indicate that vibrational convection greatly increases heat transfer rates over the unmodulated case—by 7–15% at $Gr_v = 10^5$ and by 50–65% at $Gr_v = 10^6$. The observed resonant frequencies seem to agree reasonably well with the predictions given by the resonance frequency expression derived by Fu and Shieh [*Int. J. Heat Mass Transfer* **35**, 1695–1710 (1992)]. However, this equation has been modified to include the effect of a static gravitational component and this modified equation appears to give better results when Ra and Gr_v are roughly comparable in magnitude. Copyright © 1996 Elsevier Science Ltd.

INTRODUCTION

Under terrestrial conditions, typical buoyant convective flows may disrupt sensitive crystal growth or homogeneous solidification processes. Microgravity provides a unique environment in which these bulk flows can be suppressed and more diffusive heat and mass transport mechanisms can dominate, thereby producing a variety of materials not available on Earth. Such experiments are typically very sensitive to gravitational levels and, although the mean value of gravity on these platforms may be of the order of 10^{-6}, instantaneous values of the g-level may be as high as 10^{-2} or more [1]. These higher instantaneous g-levels are due to [2]:

(1) external impacts with the spacecraft (meteorites, dockings, aerodynamic drag);
(2) mass loss from the spacecraft (dumping or rocket fringes) and
(3) crew or machinery movements within the spacecraft.

Such impulses and oscillations may induce convective flows in some experiments. A particularly interesting case occurs when the unsteady gravitational component is harmonic and stimulates convection even though the time-averaged value of this component is zero. As a result, modeling and studies of vibrational convection are useful in determining (1) the threshold of disturbances for such experiments and (2) the range of frequencies most detrimental to the experiment. In addition, such studies are of fundamental interest to heat transfer research since vibration convection may affect the stability of some systems or greatly enhance heat transfer rates. Finally, the response of such systems to oscillating gravitational fields may be of interest to those studying nonlinear dynamical systems.

Many of the works on thermovibrational convection have focused on the stabilizing or destabilizing effects of vibration on convective flows or the heat transfer enhancement due to vibrations. Sharifulin investigated the heat transfer enhancement and flow properties of the quasi-equilibrium state (defined as the condition of no time-average flow), within a horizontal cylindrical cavity [3]. Sharifulin found that at high values of the vibrational Grashod number, Gr_v, it was possible to get double-vortex flow rather than typical single vortex flow, thereby greatly increasing heat transfer rates. Ivanova and Kozlov made an experimental study of heat transfer rate enhancement between two coaxial cylinders [4]. They found that the heat transfer rate increases with non-dimensional frequency up to 600. After 600, the authors noted a slight reduction in the heat transfer rate. Forbes *et al.* made a similar experimental study with a liquid filled rectangular cavity and noted a marked increase in the heat transfer rate, up to 50% in some cases, near the resonant frequency [5].

Gresho and Sani published results of an investigation of the stabilizing/destabilizing influences of vibration on a fluid between two infinite planes at different temperatures [6]. They were interested in determining the shift due to vibrations in the critical Rayleigh number needed to induce convective motion.

NOMENCLATURE

b	vibrational amplitude
g	gravitational acceleration
Gr	Grashof number
H	cavity height
n	integer value
Nu	Nusselt number
p	pressure
P	dimensionless pressure
Pr	Prandtl number
Q	energy
r	radial coordinate
Ra	Rayleigh number
t	time
u	radial velocitry
U	dimensionless radial velocity
v	axial velocity
V	dimensionless axial velocity
z	axial coordinate.

Greek symbols

α	thermal diffusivity
β	thermal expansion
Γ	number of divisions per oscillation period
δ	phase portrait lag time
η	dimensionless axial coordinate
μ	viscosity
ν	kinematic viscosity
ρ	density
Θ	dimensionless temperature
ξ	dimensionless radial coordinate
τ	dimensionless time
ω	dimensionless frequency
Ω	frequency.

Subscripts

bottom	chamber bottom
c	cold
error	error
h	hot
i	current value
j	all other values
r	resonance
side	chamber side
top	chamber top
v	vibrational
0	reference or static case.

Their stability analyses showed that vibrations can significantly increase the stability of an unstable system or destabilize a normally statically stable system. Birigen and Peltier examined the same problem as Gresho and Sani, but considered the full three-dimensional (3D) geometry and equation nonlinearities [7]. In addition to sinusoidal modulations they also considered spatial and temporal random modulations of the g-field. Qualitatively, they arrived at the same results as Gresho and Sani and, of the temporal or spatial random modulations, they found spatial random modulations introduce more local excitations, which may be detrimental to space based crystal growth.

Upenskii and Favier studied the feasibility of using high frequency vibrations to suppress convection in a typical Bridgman-scheme crystal growth process [8]. Results indicated that, for typical semiconductor applications, magnetic field suppression would be simpler and more effective for horizontal crystal growth. In contrast, their results predicted a 10–20 times decrease in the magnitude of velocities near the crystal growth front with horizontal vibrations in a vertical Bridgman growth process over the unmodulated case.

Very few works have considered the frequency dependence of vibration systems. Many studies consider only high frequency vibrating systems where the vibration period is considerably smaller than the characteristic response time of the fluid. Under such conditions, time-averaged equations may be used to describe the system. When the vibration period is in the order of the hydrodynamic time scale, these averaged equations cannot be used and the full transient equations must be solved. Yurkov solved such a case for a 2D square cavity under-going vertical vibrations with different side wall temperatures and a linearly varying temperature distribution on the top and bottom surfaces [9–11]. Yurkov examined the frequency dependence of the average Nusselt number by calculating the Nusselt number over a range of frequencies, encompassing the resonant region. His results indicated a marked increase in heat transfer rates in the resonant region, somewhere between a dimensionless frequency of 10^2–10^3 for vibrational Grashof numbers, Gr_v ranging from 10^4 to 4.9×10^5.

Fu and Shieh made a similar study of the frequency dependence of the heat transfer rate for the classical 2D square cavity problem [12]. This study was similar to that of Yurkov, but with adiabatic boundary conditions along the top and bottom boundaries. This case was studied for a vibrational Grashof number, $Gr_v = 10^6$, and Rayleigh numbers, $Ra = 0$, 10^4 and 10^6, over a non-dimensional frequency range from 1 to 10^4. The authors divided the different frequency regimes into the five categories listed in Table 1. Like Yurkov, they found a marked increase in the heat transfer rate at the resonant frequency. In addition, they derived the following expression which may be used to predict the resonant frequency, ω_r:

$$\omega_r = \sqrt{(2Gr_v)}Pr \tag{1}$$

Table 1. Vibrational regimes as outlined by Fu and Shieh [12]

Frequency label	Characteristics
Quasi-static	Static convection dominant
Vibration convection	Static and vibrational convection comparable
Resonant	Marked increase in heat transfer rate
Intermediate	Multiple frequency phenomena
High frequency	Frequency independent response

where Gr_v is the vibrational Grashof number and Pr is the Prandtl number of the fluid. Fu and Shieh found that the predictions of equation (1) were in good agreement with their numerical results for $Gr_v = 10^6$ and also compared the equation with Yurkov's results for $Gr_v = 9\times10^4$, 1.6×10^5, 2.5×10^5 and 3.6×10^5. They found that the equation adequately predicted the resonance frequency for all the cases except $Gr_v = 9\times10^4$ in which the equation predicted a higher resonance frequency than observed.

The objective of this work is to study the heat transfer rate within a fluid-filled cylindrical enclosure subjected to vibration over a wide spectrum of frequencies. These calculations will be performed for both zero-g and terrestrial gravitational systems. Of particular interest is the heat transfer characteristics of the system at the resonance frequency of the chamber. The results for the resonant frequency will also be compared with the correlation given by Fu and Shieh [12].

PROBLEM GEOMETRY

The case considered in this work is a vertical cylinder with radius, R, equal to its height, H, filled with a Boussinesq fluid with a $Pr = 0.71$. A diagram of the problem is shown in Fig. 1. The cylinder is subjected to vertical, sinusoidal gravitational modulation such that the problem geometry is symmetric and may be considered in only two dimensions. These sinusoidal vibrations have an amplitude, b, and frequency, Ω. Therefore, the instantaneous gravitational acceleration level, $g(t)$, is made up of a static part, g_0, and a varying part, $b\Omega^2 \sin \Omega t$, or

$$g(t) = g_0 + b\Omega^2 \sin \Omega t. \tag{2}$$

The top and sides of the cylinder are considered isothermal and at a temperature, T_h, while the bottom is considered cold at T_c. At the centerline the temperature gradient is zero. All velocity components are assumed to be zero at all of the solid boundaries. At the centerline, the r component of the velocity is zero while the gradient of the z component in the direction normal to the centerline is zero.

The problem is specified by the energy, momentum and continuity equations using the following non-dimensional variables.

Dimensionless variables

$$\xi = (r/R) \quad \eta = (z/H) \quad \tau = (\alpha t/H^2)$$

$$U = (uH/\alpha) \quad V = (vH/\alpha)$$

$$\Theta = \frac{(T-T_c)}{(T_h-T_c)} \quad P = \frac{pH^2}{\rho_c \alpha^2}$$

$$\omega = \frac{\Omega H^2}{\alpha} \quad Pr = \frac{\nu}{\alpha}$$

$$Ra = \frac{g_0 \beta (T_h - T_c) H^3}{\alpha \nu}$$

$$Gr_v = \frac{[\beta b \Omega (T_h - T_c) H]^2}{2\nu^2}$$

Continuity

$$\frac{1}{\xi}\frac{\partial(\xi U)}{\partial \xi} + \frac{\partial(V)}{\partial \eta} = 0 \tag{3}$$

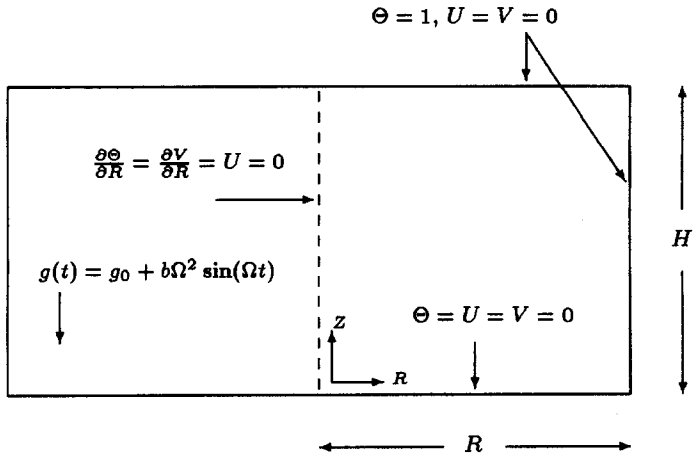

Fig. 1. Chamber geometry and boundary conditions.

Table 2. Vertical cylinder model comparison: a comparison between Nusselt numbers derived from the code used in this work and results from Huang and Hsieh for $Pr = 1.0$ and an aspect ratio of 1[15]

	$Ra = 10^2$		$Ra = 10^4$		$Ra = 10^5$	
	Huang and		Huang and		Huang and	
This work	Hsieh	This work	Hsieh	This work	Hsieh	
$\overline{Nu}_{top}$	0.3004	0.2937	0.1370	0.1576	0.0601	0.0628
$\overline{Nu}_{side}$	2.830	2.796	3.001	3.014	3.285	3.334
$\overline{Nu}_{bottom}$	5.961	5.9539	6.139	6.073	6.629	6.591

r-momentum

$$\frac{\partial(U)}{\partial\tau}+\frac{1}{\xi}\frac{\partial(U\xi U)}{\partial\xi}+\frac{\partial(VU)}{\partial\eta} = -\frac{\partial P}{\partial\xi}+Pr\left[\frac{1}{\xi}\frac{\partial}{\partial\xi}\left(\xi\frac{\partial U}{\partial\xi}\right)+\frac{\partial^2 U}{\partial\xi^2}\right] \quad (4)$$

z-momentum

$$\frac{\partial(V)}{\partial\tau}+\frac{1}{\xi}\frac{\partial(U\xi V)}{\partial\xi}+\frac{\partial(VV)}{\partial\eta} = -\frac{\partial P}{\partial\xi}+Pr\left[\frac{1}{\xi}\frac{\partial}{\partial\xi}\left(\xi\frac{\partial V}{\partial\xi}\right)+\frac{\partial^2 V}{\partial\xi^2}\right] + Pr(Ra+\omega\sqrt{(2Gr_v)}\sin\omega\tau)\Theta \quad (5)$$

Energy equation

$$\frac{\partial(\Theta)}{\partial t}+\frac{1}{\xi}\frac{\partial(\xi U\Theta)}{\partial\xi}+\frac{\partial(V\Theta)}{\partial\eta} = \left[\frac{1}{\xi}\frac{\partial}{\partial\xi}\left(\xi\frac{\partial\Theta}{\partial\xi}\right)+\frac{\partial^2\Theta}{\partial\xi^2}\right]. \quad (6)$$

These equations are solved numerically using finite differences and the SIMPLER technique. This technique has been thoroughly discussed in the literature and will not be discussed in detail here [13]. Briefly, the SIMPLER technique employs a staggered grid where pressure and temperature nodes are placed at the center of control volumes and the velocity components are positioned at the faces of these volumes. In this work the resulting discretized equations are solved using a line method and iteration for a particular time step is continued until the continuity requirement is met within a specified limit for every cell within the computational domain.

SOLUTION PROCEDURE

The code used in this work has been tested and compared with several published works, but only one example will be considered here [14]. Huang and Hsieh solved the problem shown in Fig. 1 under steady conditions using finite differences and a non-uniform 21×21 grid for $Ra = 10^2$, 10^4 and 10^5 with a Boussinesq fluid of $Pr = 1.0$ [15]. Their results included Nusselt numbers for all three surfaces of the cylindrical cavity. For an aspect ratio of 1, (i.e. $H = R$), these Nusselt numbers are defined as

$$\overline{Nu}_{top} = 2\int_0^1\left(\xi\frac{\partial\Theta}{\partial\eta}\right)\Big|_{\eta=1}d\xi \quad (7)$$

$$\overline{Nu}_{side} = \int_0^1\left(\frac{\partial\Theta}{\partial\xi}\right)\Big|_{\xi=1}d\eta \quad (8)$$

$$\overline{Nu}_{bottom} = 2\int_0^1\left(\xi\frac{\partial\Theta}{\partial\eta}\right)\Big|_{\eta=0}d\xi. \quad (9)$$

Results from the model used in this work for the identical conditions are compared with the results of Huang and Hsieh in Table 2. A 21×21 non-uniform grid was also used in this work so the results obtained in this work are not from a more refined grid. The model results compare favorably with those of Huang and Hsieh over the range of Rayleigh numbers. For reference and comparison with data later in this work, results for the static case with $Pr = 0.71$ are also given in Table 3. The cases investigated in this work are shown in Table 4. All grids were non-uniform and the numerical results near the resonant frequency were checked for a variety of grid sizes to determine a suitably refined mesh. A 21×21 grid was found to be sufficient in all cases except for $Ra = 10^5$ where a 25×25 grid was used. The choice of time step in this work was made by dividing one complete oscillation period by a value, Γ, i.e.

Table 3. Static Rayleigh number results: Nusselt number results for the vertical cylindrical cavity with $Pr = 0.71$ and an aspect ratio of 1

Ra	0	10^4	10^5
$\overline{Nu}_{top}$	0.3103	0.1383	0.06056
$\overline{Nu}_{side}$	2.804	2.979	3.263
$\overline{Nu}_{bottom}$	5.917	6.096	6.586

Table 4. Grid sizes and period divisions used in this work

	Gr_v			
Ra	10^5		10^6	
	Grid	Γ	Grid	Γ
0	21	128	21	128
10^4	21	128	21	128
10^5	25	256	25	256

$$\Delta\tau = \frac{2\pi}{\omega\Gamma}. \tag{10}$$

As in the case of the grid, the choices for Γ were made by comparing the results with larger period divisions. Values for the number of divisions for period, Γ, are also given in Table 4.

The following procedure was used for each run:

(1) choose run conditions: Rayleigh number, Ra; vibrational Grashof number, Gr_v; and frequency, ω;
(2) iterate upon condition where $Gr_v = 0$ until steady conditions are achieved—this permits identical starting conditions for all runs;
(3) when steady conditions are reached, gravitational modulations are introduced and
(4) continue run until convergence is reached.

The convergence criteria used in this work are not straightforward and will be discussed in detail. In this work, the simulation was considered converged if it met one of the two convergence criteria.

Criterion 1: *periodic response*

At the end of each sinusoidal cycle, the maximum value of the instantaneous average Nusselt number is compared with the external values of the three previous oscillations. If, for each of the surfaces of the chamber, each of these four maximum values agree within a certain degree, specifically,

$$\left|\frac{\overline{Nu}_{\max,i} - \overline{Nu}_{\max,j}}{\overline{Nu}_{\max,i}}\right| \leqslant 10^{-4} \tag{11}$$

where i indicates the maximum of the current oscillation and j represents the maxima of the three previous oscillations, then the simulation is considered converged.

Criterion 2: *multiple period or aperiodic response*

This criterion involves flows with responses which are not periodic or are periodic but have a period not equal to that of the forcing function, namely the g modulations. The solution for this case is to consider the most important quantity in the calculations, i.e. the average heat transfer rate through the system. Even if the flow is not periodic while undergoing harmonic motion, a time-averaged energy balance on the chamber must exit. Such a balance on the chamber yields

$$\frac{1}{\Delta\tau}\int_0^{\Delta\tau}(2\overline{Nu}_{\text{side}} + \overline{Nu}_{\text{top}})\,d\tau = \frac{1}{\Delta\tau}\int_0^{\Delta\tau}(\overline{Nu}_{\text{bottom}})\,d\tau \tag{12}$$

where $\Delta\tau$ is a sufficiently large sampling time. In this work a running average of the Nusselt numbers is made and the energy error, Q_{error} is defined as

$$Q_{\text{error}} = \frac{(2\overline{Nu}_{\text{side}} + \overline{Nu}_{\text{top}}) - \overline{Nu}_{\text{bottom}}}{\overline{Nu}_{\text{bottom}}}. \tag{13}$$

If the iterations were continued until the instantaneous value of the energy error was near zero, particular combinations of the Nusselt numbers could give a sufficiently small energy error before true convergence is reached. To avoid this early convergence a further test is made. At the end of each sinusoidal modulation, the root mean square of the energy error integrated over the cycle is calculated. If the r.m.s. value of the energy error is less than 10^{-3} over the course of the cycle, convergence is reached. Since all calculations start with the initial condition of no modulation, considerable error would be introduced if the running average calculations were started at the beginning of the g-modulations. Therefore, the averaging procedure is delayed by a time, $\tau = 0.15$. The choice of delay time is somewhat arbitrary—convergence can be reached with $\tau = 0$, but it may take considerably longer, computationally. A delay time of 0.15 was found to be sufficiently long transient response time for the fluid to react to the abrupt initiation of modulations.

Although somewhat elaborate and detailed, all of the runs tested reached one of the two convergence criteria. The second convergence criterion is a suitable test for any of the cases tested and criterion no. 1 is not strictly needed. However, if a flow is periodic, it will often satisfy criterion no. 1 earlier than criterion no. 2, thus saving computational time.

RESULTS

Nusselt number data

The goal of this work was to determine the average heat transfer rate through the system as a function of the vibrational frequency. To do this we have made several numerical simulations of this process over a range of frequencies and recorded the average heat transfer rate based on the convergence criteria discussed in the previous section. Figures 2 and 3 are plots of the cavity Nusselt numbers, representing the average rate of heat transfer through each surface of the chamber, as a function of the dimensionless frequency at zero-g conditions. The time-averaged Nusselt numbers for each surface of the cavity are shown by the solid curves in Fig. 2 and 3. In addition to these averages, the maximum and minimum Nusselt numbers are also given in the plot. These maxima and minima were gathered from a finite sample of oscillations before the simulation reached convergence. For cases where the flow is periodic these maxima and minima are fairly accurate. In the region where the flow is aperiodic, this finite sample may be too small to give the absolute extrema. Therefore, in the vicinity of the resonant region, the maxima and minima should be regarded only as guides in the range of oscillation in the average Nusselt number.

In Fig. 2, the average rate of heat transfer through the cavity, as given by the plot of $\overline{Nu}_{\text{bottom}}$, steadily increases with frequency until reaching a maximum at the resonance regime. After reaching this region, there

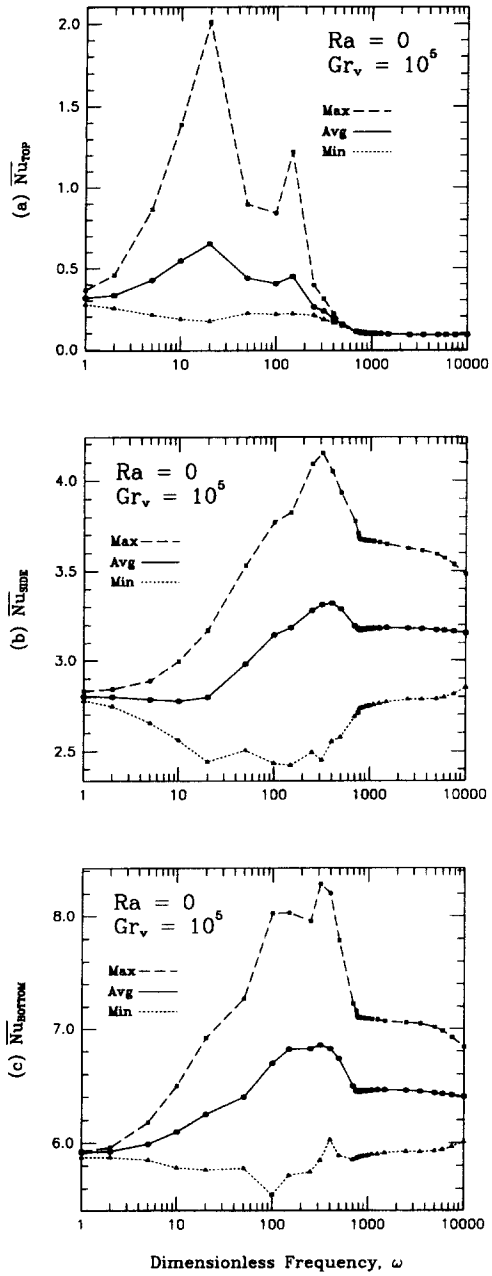

Fig. 2. Nusselt number results for $Ra = 0$ and $Gr_v = 10^5$.

is a sharp decrease in the rate of heat transfer and the average Nusselt number reaches a plateau. At this point, the average Nusselt number is relatively independent of frequency and the minima and maxima tend to converge to this average value.

The trends for $Gr_v = 10^6$ and $Ra = 0$ are similar with the following exceptions. As Gr_v is increased, the resonance region peak becomes narrower and the peak frequency is shifted farther down the spectrum.

At low frequencies, i.e. the quasistatic vibrational region, the resulting amplitudes in the average Nusselt number are small and the average Nusselt number is a relatively weak function of the frequency. At slightly higher frequencies, in the vibrational convection region, the spread between the maxima and minima begins to increase and the average Nusselt number steadily increases. Just above $\omega = 100$, the resonance region begins. In this region there is a much higher increase in the heat transfer rate and the widest spread in maxima and minima. For example, the average Nusselt number oscillates between roughly 7 and 13.5 at $\omega \sim 1000$ for $Gr_v = 10^6$.

After the resonance region, the intermediate vibrational regime is reached. In this region there is a quick decrease in the heat transfer rate until the aver-

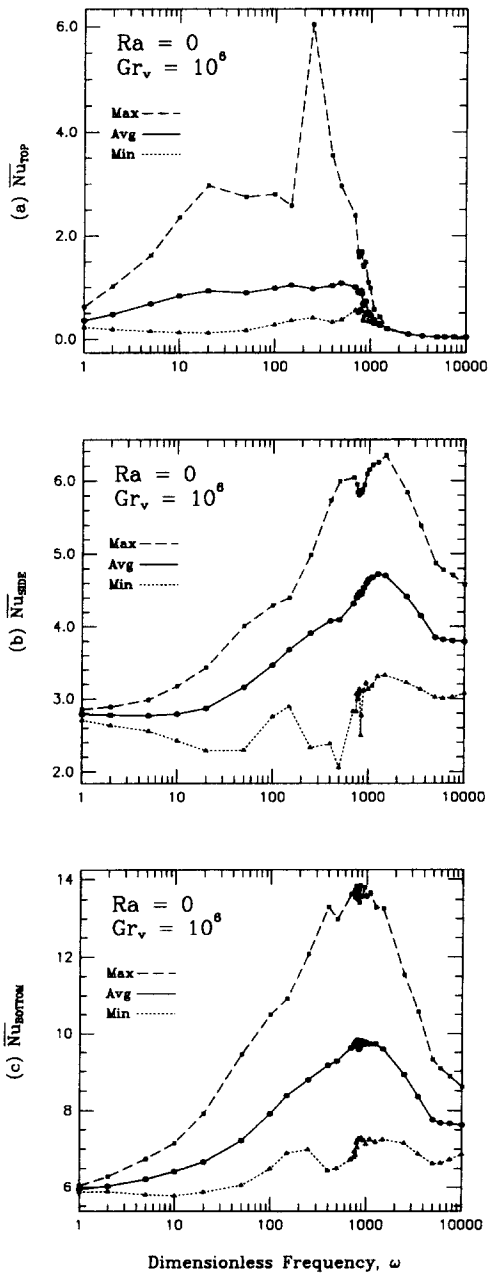

Fig. 3. Nusselt number results for $Ra = 0$ and $Gr_v = 10^6$.

age Nusselt number reaches a plateau. The intermediate regime is a transition region between the resonance and high frequency regimes. In this region, the period of vibration is becoming shorter than the hydrodynamic time scale.

At the high frequency regime, the average heat transfer rate is essentially independent of frequency and the minimum and maximum Nusselt values are gradually converging to this average. One interesting point to note is that the minima and maxima for the top Nusselt number converge to the average value rather early and that, of the high frequencies, the top is essentially adiabatic. Almost all of the heat transfer occurs between the bottom and side wall boundaries.

Figures 4 and 5 are plots of the average Nusselt numbers for $Ra = 10^4$ and $Gr_v = 10^5$ and 10^6, respectively. In these cases, the average heat transfer rate curve still follows the same trends as for the zero-g case, although the addition of the static gravitational field tends to diminish the spread in the maxima/minima at low frequencies. The average heat transfer rate is also even less dependent upon the frequency as in the zero-g case. There is a similar increase in the heat transfer rate at the resonance region; roughly 50%. These values are very similar to those of the zero-g case indicating that the resonance region is only slightly affected by the static gravitational field.

Figures 6 and 7 are plots of the average Nusselt numbers for $Ra = 10^5$ and $Gr_v = 10^5$ and 10^6. In these plots the effect of the static gravitational field tends to pervade much farther than in the previous cases, damping the fluctuation of the Nusselt number. Again, the average Nusselt number is essentially independent of frequency in this region.

In the case of $Ra = 10^5$, $Gr_v = 10^6$, there is an abrupt change in the Nu_{bottom} near the peak of the curve. A closer view of this section of curve is shown in Fig. 8. From this closer view it is easier to see the sharp drop in the Nusselt number just after the maximum heat transfer rate point is reached. Fu and Shieh found similar behavior in their work in the resonance region.

In their work Fu and Shieh started at a particular frequency and incremented/decremented the frequency, recording the data as they scanned the frequency range. They found that, near the resonance peak, they could sometimes get two different average Nusselt number curves depending upon whether the frequency was being increased or decreased. Since all the simulations in this work were started from the static, no vibrational case, it is possible that only one section of the curve is possible in this work. This type of abrupt jump is also present in the $\overline{Nu}_{\text{bottom}}$ cases of Figs. 3(c) and 5(c).

Frequency response

A more detailed analysis of the frequency response of the system to the gravitational modulation yields some interesting phenomena. Figure 9 is a plot of the response of the average Nusselt number over time for

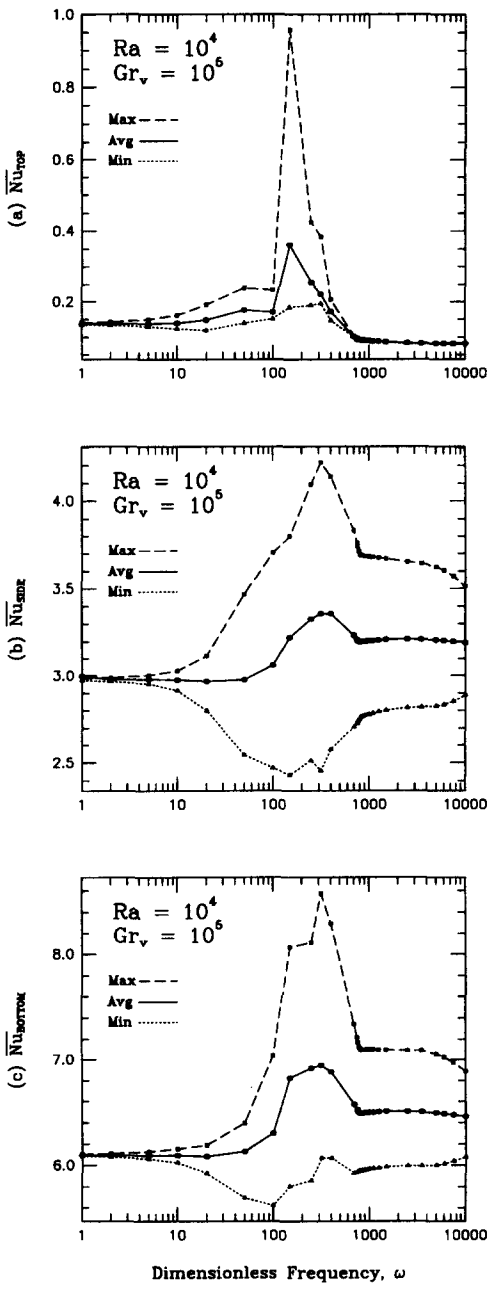

Fig. 4. Nusselt number results for $Ra = 10^4$ and $Gr_v = 10^5$.

five distinct frequencies. In each case, the response of the bottom boundary Nusselt number to 100 cycles of the gravitational modulation is shown along with phase portraits for each frequency. These data were collected from the $Ra = 0$ and $Gr_v = 10^6$ case only, but the data for the other conditions show similar behavior. The phase portraits in Fig. 9 were generated by plotting the value of the Nusselt number with a 1/4 period phase lag against the unlagged value of the Nusselt number.

The response to a nondimensional frequency of 100 is shown in Fig. 9(a). This response is within the vibrational convection region where the static and

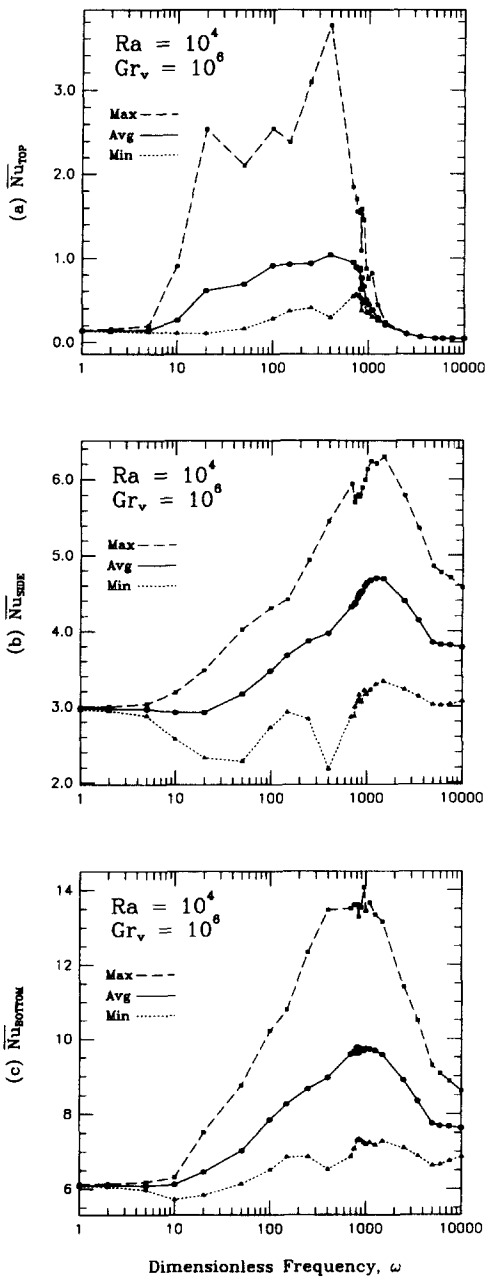

Fig. 5. Nusselt number results for $Ra = 10^4$ and $Gr_v = 10^6$.

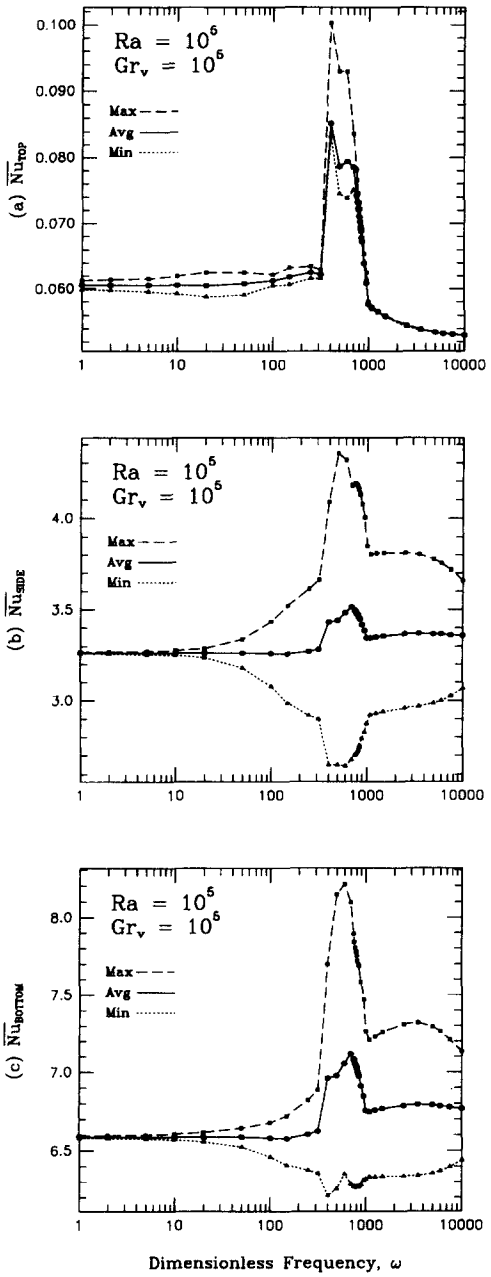

Fig. 6. Nusselt number results for $Ra = 10^5$ and $Gr_v = 10^5$.

vibrational convection are of comparable magnitude. There is a simple, periodic response to the forcing function as shown by the single, simple closed loop in the phase portrait.

As the frequency increases the response becomes more complex. The region with $\omega = 850$ is representative of the resonance region. In this region the heat transfer rate does not consist of simple, single periods. Instead, it has a period-4 response as shown by the four lobes of the phase portrait.

The results for $\omega = 1000$ are even more complex than for $\omega = 850$ even though it only represents a modest increase in the frequency and the results are still in the resonance regime. Characteristics of frequencies less than the period of the forcing function have appeared. Also the response as shown in the phase portrait is much more complex. There are many more lobes than in the plot for $\omega = 850$, but these lobes appear to be banded. The banded structure of the phase portrait suggests that the response is still a period-n response, but n is very large in this case.

The response for $\omega = 2500$ is also very interesting. The oscillations in the Nusselt number seem to have a period comparable to that of the forcing function and the amplitudes are nearly the same, yet these amplitudes are all slightly different and there is no

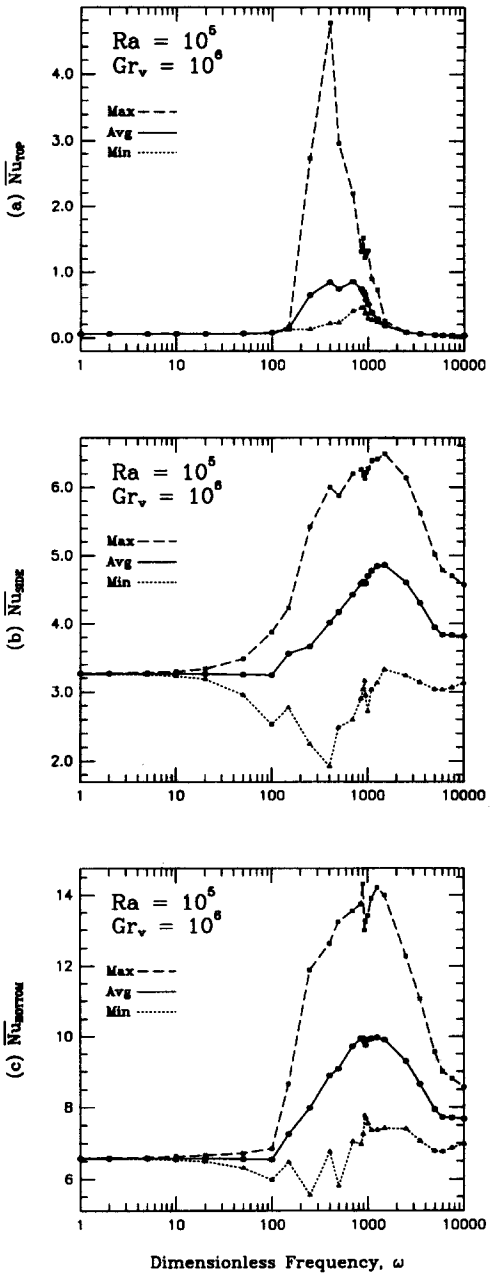

Fig. 7. Nusselt numbers results for $Ra = 10^5$ and $Gr_v = 10^6$.

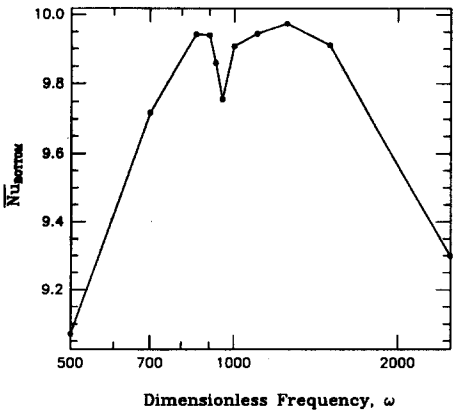

Fig. 8. "Jump" phenomenon: a closer view of the resonance region for $Ra = 10^5$, $Gr_v = 10^6$ and the abrupt dip in the Nusselt number curve.

apparent repeating pattern in these oscillations. There are also no distinct bands in the phase portrait for $\omega = 2500$, and the phase portrait loops appear to be evenly distributed within a closed region. This type of response is characteristic of chaotic flows. Although it cannot be conclusively stated whether this particular case is chaotic, the evidence gathered thus far indicates that this may be a possibility.

Finally, the response to $\omega = 10\,000$ is shown in Fig. 9(e). As the frequency is increased to this high frequency regime, the Nusselt number response again returns to simple, harmonic response as shown by the single, closed loop in the phase portrait.

Resonant frequency

In this work the resonance frequency was assumed to be the frequency where the energy transfer rate through the cavity was maximized. Table 5 is a list of these maxima for the six conditions studied in this work. Since information is only available from a limited number of discrete frequencies, the maximum value is given along with a range of frequencies which bracket this maximum. The range boundaries fall within approximately 1% of the maximum energy transfer rate.

Table 5 also shows the percentage increase in the heat transfer rate at the resonant frequency over the static, nonvibrational case. As shown in the table the resonant oscillations greatly enhance the heat transfer rate through the system. The greatest increase occurs for the zero-g or $Ra = 0$ case. As the Rayleigh number is increased the differences between the modulated and unmodulated cases begin the shrink. Nevertheless, for the $Gr_v = 10^6$ cases studied in this work there is a 50–65% increase in the heat transfer rate at the resonant frequency. The increases for the $Gr_v = 10^5$ cases are more modest and range from 7 to 15%.

According to equation (1) the resonance frequency should be 318 and 1004 for $Gr_v = 10^5$ and 10^6, respectively. These predictions seem to agree only with the results for the cases of $Ra = 0$, $Gr_v = 10^5$ and $Ra = 10^4$, $Gr_v = 10^5$. For example, the numerically derived resonance frequencies for both $Ra = 0$, 10^4 and $Gr_v = 10^6$ fall roughly 200 points below the predictions of equation (1). The resonance frequencies in Table 5 have been chosen because the energy transfer rate is maximized at these points. This definition, though undoubtedly close to the resonant frequency, may not represent the true resonant value. As such, the frequency ranges which bracket these maxima have also been included in this table. In these two cases the resonance peak/ranges are broad and are nearly centered on the values predicted by equation (1). The only exception to this is the data for $Ra = 10^5$. Both the numerically derived resonance frequencies

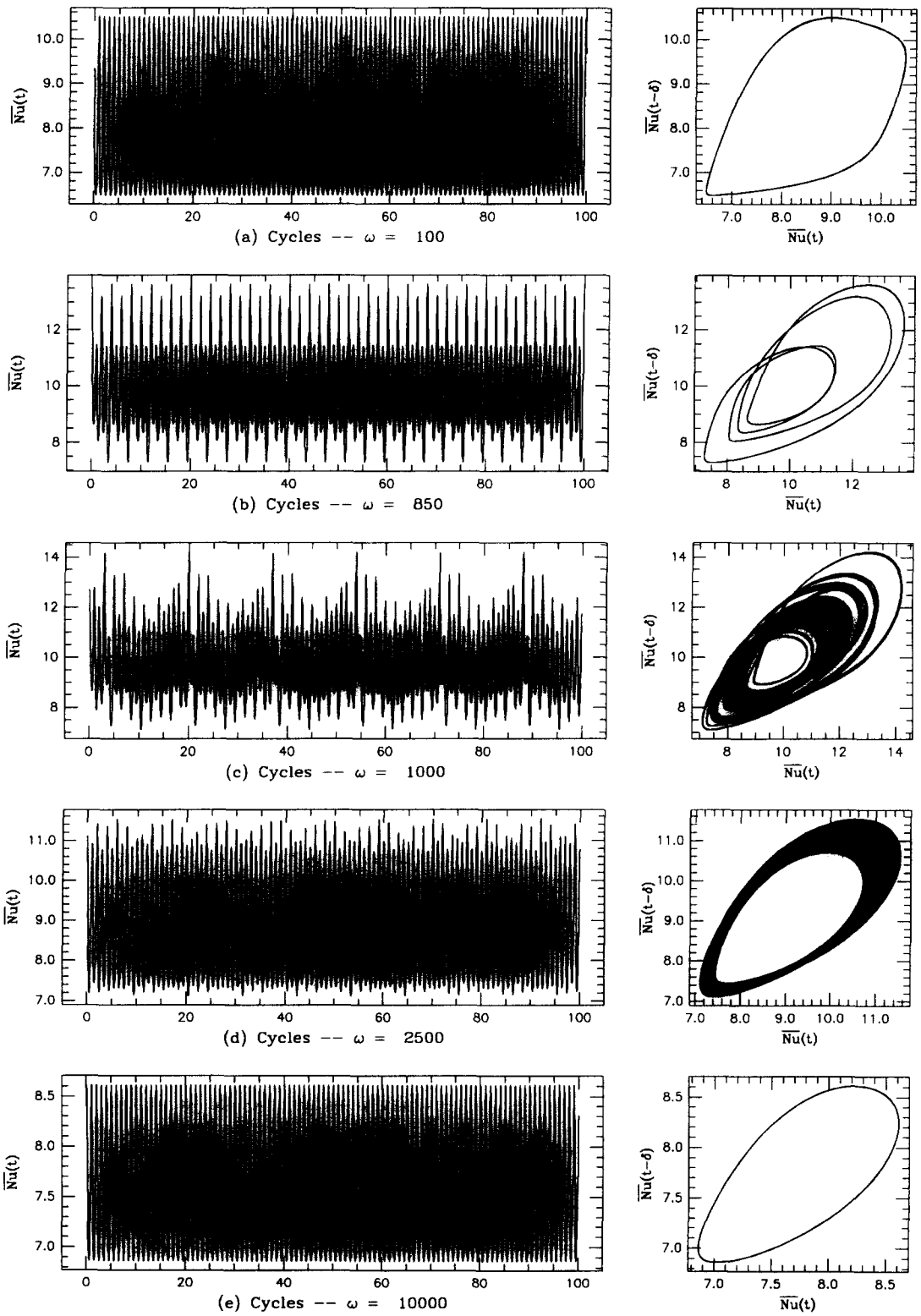

Fig. 9. Representative frequencies and phase portraits: the figures on the left are plots of $\overline{Nu}_{\text{bottom}}$ over the course of 100 gravitational oscillations; the phase portraits on the right are plot of $\overline{Nu}_{\text{bottom}}$ with a 1/4 period phase lag, δ, plotted against the unlagged value of $\overline{Nu}_{\text{bottom}}$.

Table 5. Resonance frequency results

Ra	Gr_v	ω_r observed	$\overline{Nu}_{bottom}$ at ω_r	Percentage increase in heat transfer rate	Frequency range	ω_r from equation (1)	ω_r from equaiton (15)
0	10^5	318	6.85	14.7	136–445	318	318
0	10^6	810	9.83	64.5	772–1153	1004	1004
10^4	10^5	318	6.95	12.8	206–405	318	404
10^4	10^6	825	9.78	58.9	778–1259	1004	1038
10^5	10^5	700	7.12	7.0	591–789	318	771
10^5	10^6	1250	9.97	49.9	804–1560	1004	1278

and ranges are significantly higher than the results predicted by equation (1).

One possible explanation for the discrepancy could be that the effects of the static Rayleigh number on the resonant frequency have become more significant at $Ra = 10^5$. In deriving the relationship for the relationship for the resonant frequency, Fu and Shieh reasoned that the inertial terms were comparable to the buoyancy terms, or

$$\frac{dv}{dt} \sim b\Omega^2\beta\Delta T \sin\Omega t + g\beta\Delta T. \tag{14}$$

They also reasoned that the resonant frequency is only slightly affected by the static gravitational term and dropped the second term in the right hand side of equation (14) from their derivation. If this term is included in the derivation the result is a quadratic equation with the following solution:

$$\omega_r = \frac{\sqrt{(2Gr_vPr^2)} + \sqrt{(2Gr_vPr^2 + 2\pi^2 RaPr)}}{2}. \tag{15}$$

Equation (15) reduces to equation (1) for $Ra = 0$ and the effect of the static Rayleigh number on the resonance frequency is trivial at low values of the static Rayleigh number, reinforcing the assumption made by Fu and Shieh. For $Gr_v = 10^5$–10^6, as studied in this work, the value of the resonance frequency is relatively unaffected until reaching the range of $Ra = 10^5$. Equation (15) predicts an increase in the resonance frequency with higher static Rayleigh numbers and a comparison between equation (15) and the numerical results from this work is shown in Table 5. Equation (15) gives the same reasonable agreement for the $Ra = 0$ or 10^4 cases, but it gives better agreement for the $Ra = 10^5$ case over equation (1).

CONCLUSIONS

We have presented a model of thermovibrational convection in a vertical, cylindrical cavity and studied the frequency dependence of the heat transfer rate through the system at several Rayleigh and vibrational Grashof numbers. In addition, a great deal of attention has been focused on the energy transfer rate at the resonant frequency of the cavity. In the resonant regime, the thermovibrational case gave a 50–65% higher heat transfer rate at $Gr_v = 10^6$ and a 7–15% higher heat transfer rate at $Gr_v = 10^5$ over the static, unmodulated case. The results of this work are similar to the results obtained by Fu and Shieh, but, unlike their work, the geometry in this case consisted of multiple surfaces for heat transfer. Most of the energy transferred in the system occurred between the side wall and the bottom surface. This is especially true at high frequencies where the top of the cavity can become virtually insulated. This result is similar to what occurs for the static case at high Rayleigh numbers [15]. Finally, equation (1) derived by Fu and Shieh is a useful means of estimating the resonance frequency at low static Rayleigh numbers. However, this equation has also been extended to include the effect of the static gravitational field on the resonance frequency and it appears that equation (15) may be more suitable for cases where the Rayleigh number and vibrational Grashof number are somewhat comparable in magnitude.

A closer view of the response of the system to increasing frequency has also shown some interesting results. At low frequencies the heat transfer rate response to vibrations is a simple, period-1 response. As the resonance region is approached, this response seems to remain periodic but increases in complexity. Just above the resonance frequency, the flow becomes very complex and it appears that the Nusselt number response is chaotic. Finally, as the high frequency limit is approached, the flow returns to a simple periodic response. A more detailed study of these different regimes and the possibility of a chaotic response will be the subject of future work.

Acknowledgements—We would like to gratefully acknowledge support for this research under the National Research Council's Research Associate Program.

REFERENCES

1. Walter Knabe and Dirk Eilers, Low-gravity environment in spacelab, *Acta Astronautica* **9**, 187–198 (1982).
2. R. Monti, Gravity jutters: effects on typical fluid science experiments. In *Low-gravity Fluid Dynamics and Transport Phenomena* (Edited by Jean N. Koster and Robert L. Sani), Chapter 4. American Institute of Aeronautics and Astronautics, Washington, D.C. (1990).
3. A. N. Sharifulin, Supercritical vibration-induced ther-

mal convection in a cylindrical cavity, *Fluid Mech.—Sov. Res.* **15,** 28–35 (1986).
4. A. A. Ivanova and V. G. Kozlov, Vibrationally gravitational convection in a horizontal cylindrical layer, *Heat Transfer—Sov. Res.* **20,** 235–247 (1988).
5. R. E. Forbes, C. T. Carley and C. J. Bell, Vibration effects on convective heat transfer in enclosures, *J. Heat Transfer* **92,** 429–438 (1970).
6. P. M. Gresho and R. L. Sani, The effects of gravity modulation on the stability of a heated fluid layer, *J. Fluid Mech.* **40,** 783–806 (1970).
7. S. Birigen and L. J. Peltier, Numerical simulation of 3D Bénard convection with gravitational modulation, *Physics Fluids A* **2,** 754–764 (1990).
8. V. Upenskii and J. J. Favier, High frequency vibration and natural convection in Bridgman-scheme crystal growth, *Int. J. Heat Mass Transfer* **37,** 691–698 (1994).
9. G. Z. Gershuni and Ye. M. Zhukhovitskiy, Vibration-induced thermal convection in weightlessness, *Fluid Mech.—Sov. Res.* **15,** 63–84 (1986).
10. Yu S. Yurkov, Vibration-induced thermal convection in a square cavity in weightlessness at arbitrary frequencies, *II Vsesoyuznyye seminar po gidromekhanike i teplomassoobmenu v nevesomosti*: [*Tezisy dokladov*], Perm, 36–37 91981). As cited in ref. [9].
11. Yu S. Yurkov, Vibration-induced thermal convection in a square cavity in weightlessness (finite frequencies), *Konvektivnyye techeniya* (convective flow), Perm Teacher's Institute. Perm, 98–103 (1981). As cited in ref. [9].
12. W. S. Fu and W. J. Shieh, A study of thermal convection in an enclosure induced simultaneously by gravity and vibration, *Int. J. Heat Mass Transfer* **35,** 1695–1710 (1992).
13. S. V. Patankar, *Numerical Heat Transfer and Fluid Flow*. Hemisphere, Washington, D.C. (1980).
14. Frank T. Ferguson, Numerical simulation of natural convective flows within a nucleation chamber under variable gravity. Ph.D. Thesis, University of Virginia, Charlottesville, VA (1993).
15. D. Huang and S. Hsieh, Analysis of natural convection in a cylindrical enclosure, *Numer. Heat Transfer* **12,** 121–135 (1987).